Ultrathin Alumina Film Al-Sublattice Structure, Metal Island Nucleation at Terrace Point Defects, and How Hydroxylation Affects Wetting

D. R. Jennison[#] and A. Bogicevic
Surface and Interface Sciences Department 1114
Sandia National Laboratories, Albuquerque, NM 87185-1421 USA

_____

First principles density-functional slab calculations have produced the following results: 1) For 5 Å (two O-layer) alumina films on Al(111) and Ru(0001), with larger unit cells than in recent work, the lowest energy stable film was found to have an even mix of tetrahedral (*t*) and octahedral (*o*) Al ions arranged in alternating zig-zag rows. This most closely resembles the κ-phase of bulk alumina, where this pattern results in a greater average lateral separation of Al-ions than with pure *t* or *o*. A second structure with an even mix was also found, consisting of alternating stripes. These patterns can exist in any of three equivalent directions on close packed substrates. 2) Because of numerical problems associated with the very large relaxations in alumina surfaces, MgO(100) was used to investigate metal island nucleation. Common point defects (vacancies, pairs of vacancies, and water by-products) were placed in supercells and their effects on Pt adatom and ad-dimer binding computed. Unexpectedly, single vacancies were found to **de**stabilize metal dimers, and only the mixed (F_s-V_s) divacancy increases stability. Among the water by-products, in-surface OH (produced by H^+ reaction with O^{2-}) was uninteresting, but ad-OH was found to both increase adatom binding and significantly stabilize dimers on the surface, suggesting the latter defect nucleates metal islands even at elevated temperatures. We believe these results apply to all highly ionic oxides. 3) Finally, the effect of a substantial coverage of hydroxyl on Cu deposition and growth on α-Al_2O_3(0001) was investigated. While Born-Haber calculations show wetting is not thermodynamically preferred on the clean

_____

[#]To whom correspondence should be addressed.
email: drjenni@sandia.gov

surface, at experimentally relevant ad-OH coverages the strength of the Cu/oxide bond is more than doubled and wetting is strongly favored. This causes a very stable ~1/3 ML coverage of Cu^{+1}, which then induces layer-by-layer Cu growth, in agreement with recent experiments. Hydroxyl coverage can thus control deposited metal morphology across a wide spectrum.

---

1 Introduction

In this paper, we include for discussion three topics of current interest in metal oxide surface science. Using first principles density functional theory (DFT) [1] calculations, we have investigated: 1) the atomic-scale structure of experimentally-relevant ultrathin alumina films, 2) the role of common point defects in metal island nucleation on oxide terraces, and 3) the growth and morphology of metals on oxide surfaces which have high concentrations of a common impurity.

1.1. Ultrathin Alumina Film Structure

Aluminum oxide films have a substantial focus for a variety of reasons. First, they represent structures which may be produced during the oxidation of Al metal, and are thus important for understanding the "barrier layer" which inhibits corrosion. Second, thin films enable the study of adsorption without the charging and hydrogen impurity problems which plague bulk-terminated Al_2O_3. Third, since alumina is an important support material, when metal nanoclusters/crystals are produced by metal deposition, the films serve as model catalysts [2]. Finally, there is growing interest for microelectronics applications.

Considerable experimental and theoretical work on this system has occurred recently, with a main topic being metal adsorption and the islands which result [3]. Obviously, nucleation plays a critical role here (see below), but without a knowledge of atomic scale structure one cannot address the first

issue, the basic energetics of adsorption, diffusion, and dimer stability.

Two O-layer 5 Å films are of particular interest because this thickness appears to be self-limited when produced by NiAl(110) [4] or Ni$_3$Al(111) [5] oxidation, and more recently by the deposition and subsequent oxidation of Al on Ru(0001) [6]. (Two-layer oxide films have also been recently seen in a completely different system: encapsulated Pt nanocrystals on TiO$_2$ [7].)

HREELS evidence from Al$_2$O$_3$/NiAl(110) suggests a mixture of octahedral (*o*) and tetrahedral (*t*) Al ions is present [8], which has resulted in the films being called "gamma-like". Recently, TEM Moire patterns have indeed indicated that the lattice constant of the film is consistent with γ-phase [9], but this result is also consistent with other possible structures. (Of course, film thinness, at two O-layers, prevents a definable hcp vs. fcc stacking which differentiates the α- and γ-phases.) Actual structural details are in fact unknown, but a significant hint has arisen from new experiments by the group of Behm [6] on Al deposition and subsequent oxidation on Ru(0001). While islands of 5Å thick Al$_2$O$_3$ were seen at various coverages using STM, LEED evidence for ordering in the Al sub-lattice was *not* or only weakly seen, in spite of annealing well above 300K.

On the theoretical side, recent calculations on two and three O-layer Al$_2$O$_3$ films on Al(111), Mo(110) and Ru(0001) produced three significant findings [10]: 1) the preferred interface between the oxide film and the substrate metal consists in all cases of 1x1 chemisorbed oxygen, 2) on top of which is a nearly coplanar layer of Al and O ions, 3) with the normal bulk preference for octahedral-(*o*) over tetrahedral-site (*t*) aluminum ions energetically reversed. The last result is due to the electrostatics and layer separations induced by the interface with the underlying metal. However, this initial work used only small unit cells, and did not allow for the possibility of greater complexity. Here, we report computational results obtained by expanding the unit cell to allow a variety of *t*/*o* ratios and structures.

1.2 Metal Island Nucleation on Terraces

Surface topographs from scanning-tunneling microscopy (STM) or atom force microscopy (AFM) observe metal island nucleation on oxide surfaces not only at line defects (such as antiphase domain boundaries [4, 11] and steps [12], where metal atoms presumably bind more strongly and therefore have a tendency to collect and meet) but also on terraces. For the latter, nucleation could of course occur on a perfect surface, depending on the temperature and density of the adatom lattice gas (which determine the stability of metal ad-dimers, the probability of attaching a third metal atom, etc.). In contrast, surface defects might dominate nucleation in experimental conditions [2, 13-16].

Even though it has been speculated that the most common defect in well prepared surfaces, specifically isolated surface oxygen vacancies [17], may act as nucleation sites [13, 14], this has not been substantiated via experiment or theory. Here, we report an investigation of the influence of surface vacancies on Pt island nucleation [18]. For completeness, we also examined how water dissociation products affect nucleation, since there have been several reports that these are common low density contaminants on prepared oxide surfaces [17, 19].

It is very difficult numerically to study these defects in alumina films or with sapphire because of the extremely large surface relaxations [20, 21]. Therefore, we have chosen a system with an order-of-magnitude smaller relaxations [21], MgO(100). From this first study of dimer stability at oxide surface defects, several findings are completely unexpected, but are really quite intuitive in retrospect, and are likely to be general for highly ionic oxides.

1.3 How Hydroxylation Affects Wetting

Cu deposition on oxides has assumed increased recent importance because of microelectronics applications. However, experimental results [22-27] for Cu on alumina have been inconsistent. XPS

studies [22] of Cu deposited by thermal evaporation onto bulk truncated α-Al_2O_3(0001) indicated ordered layer-by-layer growth for the first 2-3 atomic layers. The initial Cu ad-layer was observed as oxidized Cu, in the form of Cu(I) ions. Other studies on polycrystalline Al_2O_3 reported layer-by-layer growth [23] and Cu(I) formation at coverages below 0.5 monolayers [24]. In contrast, a study on epitaxial ~ 20 Å Al_2O_3 films formed on refractory metal substrates [25] reported the growth of 3-dimensional clusters of metallic Cu, even at submonolayer Cu coverages. In particular, XPS and low energy ion scattering (LEIS) [25] indicated Cu cluster formation at the lowest observable coverages at both 300 K and 80 K, with no Cu(I) observed. In addition, XANES [26] measurements carried out on sapphire substrates have reported no evidence of Cu oxidation, and coverage-dependent shifts in Cu core level and LMM peaks have been interpreted in terms of final state screening [27], rather than ionization of the Cu. Meanwhile, recent ion scattering experiments by Ahn and Rabalais [19] have shown that cut and polished sapphire(0001) surfaces (the basal plane is not a cleavage surface) cannot be made free of hydrogen contamination in the form of hydroxyl, even by annealing to 1400K. Finally, experimental studies of Rh deposited on ultrathin epitaxial Al_2O_3 films [28] suggest that surface hydroxyl binds the Rh to the surface as a cation and serves as nucleation sites for Rh clusters. These studies have raised the issue of the role of surface hydroxyl groups in producing the apparent disagreements summarized above.

The most recent experimental work, by Kelber et al. [29], indicates initial layer by layer growth of Cu on hydroxylated α-Al_2O_3(0001) at 300K, and the exclusive presence of Cu(I) during the formation of the first layer. Analysis of x-ray excited Cu(LMM) Auger data indicates that changes in the spectra are due to changes in the initial electronic state of the copper rather than to final state screening effects. The degree of surface hydroxylation is estimated to be high, ~ 1/3 ML (here, 1 ML means one adsorbate per surface O-ion), on the basis of O(1s) XPS, consistent with Ref. [19].

In collaboration with Kelber et al. [29], we have computed the adsorption energy of Cu at 1/3 and 1 ML coverages, both on clean α-Al_2O_3(0001) and on α-Al_2O_3(0001) with 1/3 ML of ad-OH. Born-

Haber cycles were then used to study the relative energy of isolated adatoms vs. incorporation into 2D islands. We find dramatic effects on the binding energies due to hydroxylation and also on the growth mode, suggesting that hydroxylation may explain the discrepancies in the experimental record.

Following a description of the computational details, we present our results and raise some issues for future work and for discussion.

2 Computational Method

Our electronic structure calculations were performed using the Vienna *Ab initio* Simulation Package (VASP) [30]. This plane-wave based density-functional code uses the ultra-soft pseudopotentials of Vanderbilt [31], which have good convergence for these systems with a plane wave cutoff of only ~ 270 eV. We used either the "standard" local density approximation (LDA) [32] or the PW91 GGA [33], as indicated below. The geometric relaxation was done first with a quasi-Newton algorithm using computed interatomic forces. For the alumina systems, where relaxation is large and problematic because of a mix of very hard and soft modes, geometry was refined with a damped dynamics scheme built into VASP. The vacuum gap was in all cases >18 Å, and k-point sampling was tested to ensure convergence to the quoted level of accuracy.

2.1 Ultrathin Alumina Film Structure

Our slabs had the alumina film on 4-7 layers of Al(111) or Ru(0001). The x-y dimensions of the supercell depended on the structure being studied. Because LDA has shown excellent accuracy in alumina structural predictions [20] and GGA does not improve on same [34], LDA was used here.

Since our study necessitated numerous computations using large supercells, the following tests were performed to ensure accuracy: 1) The relative energies of 2x1 supercells (Fig. 1, top) with *-o-o-, -t-o-,* and *-t-t-* zig-zag Al-rows were computed for a film with seven layers of Ru substrate (bottom four frozen at bulk LDA spacings) and using eight k-points. Errors produced in *relative* energy by reducing the Ru slab to just four layers (bottom two frozen), and/or the number of k-points to two, were found to be < 0.1 eV out of energy differences of ~ 2 eV per 2x1 cell. 2) Because numerical noise (arising from small inaccuracies in force computation) is seen to grow significantly during prolonged geometric relaxation, tests were done to examine the effect of freezing the entire metal substrate (these systems mix strong and soft vibrational modes, and all first-guesses had ions at the ideal positions with respect to the extended metal lattice). It was again found that errors were small, here below 0.05 eV per 2x1 cell. These results indicate that the relative energies are determined almost entirely within the oxide film itself which, because the bands are relatively flat, can be described adequately by few k-points.

2.2 Metal Island Nucleation on Terraces

A supercell of five MgO(100) layers with 36 atoms each was used together with GGA [18]. Two types of OH impurity were studied: as a "neutral" species it is produced by adding OH or H to the supercell, while as a "charged" species it occurs when both OH and H are added to the supercell, which naturally charge separate into ad-OH$^-$ and H$^+$, the latter reacting with a surface O^{2-} to produce in-surface OH$^-$. The latter was found to reduce the binding of ad-Pt atoms (due to the reduction in charge compared with the perfect surface) and are thus uninteresting for nucleation, except as a means to concentrate the density of Pt adatoms in defect free regions; we do not discuss them further. Except at the highest coverages, because of its large electron affinity ad-OH would exist as a negative ion rather than as a radical.

2.3 How Hydroxylation Affects Wetting

The sapphire slab had nine O-layers of one Al_2O_3 unit each, for 45 atoms per unit cell, as was used in a previous study [20]. In order to compare with previously published metal adsorption energies [20, 21], LDA was used for these calculations. The initial Cu positions were at the most favored sites, which at 1/3 ML coverage are atop the deepest lying Al-ion, and at 1 ML coverage are atop O. The ad-OH was placed initially at the most favored site also, atop the shallowest Al-ion. Relaxations were small laterally, thus preserving these site descriptions for the relaxed geometry.

3 Results and Discussion

3.1 Ultrathin Alumina Film Structure

In order to consider only the energetically lowest-lying possibilities, we impose three constraints: 1) We do not allow for non-stoichiometry in the Al/O ratio; 2) We restrict coordination to what is normal, i.e., each surface O has two nearly coplanar [10] Al nearest neighbors; and 3) We do not consider geometries where *t* and *o* ions are in sites which are immediately adjacent.

Our analysis indicates it is not possible to produce a localized *o*-containing "defect" starting with all *t*-ions, or visa versa, without violating the above restrictions. However, it is possible to produce a zig-zag row of *o*-ions embedded in an otherwise perfect film of 100% *t*-ions by displacing a row laterally (in the vertical direction in Fig. 1) so as to move all the ions in that row from *t* to a neighboring *o* site. Note that the effect of such a movement is to increase locally the average Al-Al interatomic spacing. Thus this electrostatic advantage, maximized by an alternating mixture of *t* and *o* rows (i.e., *-t-o-t-o-*), competes with the *t* site preference, reported in Ref. [10].

Table I shows the relative energies of the pure *o* and *t* structures compared with the even mix zig-zag

structure on both Al(111) and Ru(0001) substrates. We find for both systems that the lateral electrostatic advantage of alternating *o* and *t* dominates over the *t*-site advantage. A second type of *-t-o-* evenly mixed structure has also been found, consisting of alternating stripes (see Fig. 1, bottom). It is also noted that this structure can mix with the zig-zag one, producing a displacement in the zig-zag axis. However, we find for Ru(0001) that the striped structure is significantly higher in energy than the zig-zag, even though the Al-Al nearest neighbor spacings are the same to several neighbor shells.

It is now obvious that it is also possible to have any mix of the two types of rows. For example, the even zig-zag mixture, with *-t-o-* alternating rows, has a 2x1 unit cell (Fig. 1, top), relative to the primitive cell of three O- and two Al-ions in the surface plane of the film. Additionally, the 3:1 ratio of ion types then has a 4x1 cell (e.g., *-t-t-t-o-*), but the 2:1 ratio results in a 6x1 cell because of the reversal of the phase of the zig-zag after a single *-t-t-o-* sequence. Thus far, we have been unable to converge these other films geometrically as flat structures. Instead, computationally the energy lowers monotonically as 3D stripes (three oxygen layers thick) are produced, separated by depleted regions. In other words, the additional degrees of freedom allowed by the larger unit cells permits the geometry relaxation algorithm to find structures which, while overall energetically preferred, are perhaps not relevant to the (actually metastable) flat structures produced experimentally. Work here is continuing.

If it were not for the effects of relaxation, the relative energies of various mixes could be modeled easily. If short range row-row interactions were to dominate, the cost of converting an *o*-row into a *t*-row or a domain of the perfect 2x1 structure, *-o-t-o-t-o-t-*, into one with reversed phase on the right, *-o-t-t-o-t-o-* could be estimated as follows: 1) A reduction in energy of ~ 0.2 eV per primitive cell for each extra *t*- vs. *o*-row (see Table I and Ref. [10]); and 2) A penalty of ~ 1.0 eV per primitive cell (for Ru(0001) substrates, Table I) for each *t-t* nearest row-row interaction instead of *t-o*.

The net cost of phase reversal or other deviations from the 2x1 structure would be lowered by relaxation and further-than-nearest row-row interactions. These make it possible that the actual energetic cost may be sufficiently low that real films, where local structure is also influenced by defects and film growth conditions, may display a loss of long range order in the Al-sublattice by this phase-reversal mechanism. Another possibility for such a loss is presented by the striped structure, in that a small inclusion of stripe between two zig-zag portions results in the zig-zag shifting laterally. Here too, the large relaxations inherent in alumina would reduce the cost of such a defect below that estimated on the basis of the perfect structures (Table I). Without calculations with very large relaxed supercells, it is difficult to predict the actual energetics.

It seems likely that the 2x1 zig-zag dominates in real films (as the lateral Al-Al repulsion is minimized). Domains would then be determined by surface features, such as linear defects, and by film nucleation and growth. While a loss of long range Al-sublattice order would cause an amorphous appearance in scattering experiments such as LEED, the film is still locally dense and its adsorption properties little affected since the surface sites are so similar locally.

Even though our calculations were done using the experimentally relevant substrate of Ru(0001), since the calculations on Al(111) show qualitatively similar results, we suggest these likely apply also to films grown on NiAl [4] and Ni_3Al [5], as no Ni rises into the film and the film/substrate interface, which drives the film structure, is thus similar to having chemisorbed 1x1 oxygen on Al(111).

Of all known aluminum oxide bulk phases, the 2x1 zig-zag (Fig. 1, top) most closely resembles the so-called A plane of κ-Al_2O_3 [35] (recently structurally determined entirely by DFT and in close agreement with X-ray scattering from CVD-grown samples). This phase has -A-B-A-C- bulk stacking of the close packed near-hexagonal O layers, and the A plane has an even mixture of o and t, arranged in the alternating zig-zag rows (Fig. 1, top), while the B and C planes have all o-ions [35].)

If the 5 Å films indeed prefer the A plane structure, one may speculate that this would nucleate κ-like alumina films if grown thicker.

3.2 Metal Island Nucleation on Terraces

In Fig. 2, we find the results of our study. Because water contamination is an issue, we initially studied water adsorption and dissociation, finding it will not dissociate on the perfect surface [15, 36] but when it does dissociate (either due to defects or to solvation [36]) it does so as separated ions (Fig. 2, left column — favored structures are always towards the top of Fig. 2). Next, we see the effects of vacancies and water products on Pt adatom binding, noting a general increase in binding due to the presence of hydroxyl (Fig. 2, center column). Finally, we note the effects of defects on Pt ad-dimer stability (Fig. 2, right column). Of the vacancies, only the mixed divacancy increases the dimer binding, while the ad-OH species both increase same significantly. Note at moderate ad-OH concentrations, one might expect the charged species to be present, which has the greatest effect on dimer stability.

These results may be simply understood. When a Pt adatom encounters a vacancy of either type, it is drawn to it and becomes ionized by the Madelung potential. It enters the vacancy to the extent allowed by its ionic radius. Because it is an ion, its ability to bind to a second Pt atom is largely destroyed (and is repulsive in the LDA approximation). These results should hold for ionic oxides, all having substantial Madelung potentials. With ad-OH$^-$, however, a Pt adatom and ad-dimer find themselves at a "mini-step", with attractive electrostatic interactions both vertically (to the underlying O^{2-} ions) and laterally (to the OH$^-$).

3.3 How Hydroxylation Affects Wetting

In Table II, we see that on perfect sapphire(0001), Cu binds less than half as strongly as on the hy-

droxylated surface. In particular, the increase in adatom binding (represented by 1/3 ML) not only reverses the preference for wetting given by the Born-Haber cycle, but also pins the Cu adatoms so they are immobile up to very high temperatures (>1000K) and are unable to reach and join 3D islands, presumably nucleated at defects such as steps. This pinning is caused by the large loss of binding energy that would occur were a Cu atom to move laterally away from the adjacent OH, which it sits next to in the relaxed geometry. In the Born-Haber calculation, the tendency to form 2D islands vs. separated adatoms is given by $\Delta E = E(1ML) + 2E(slab) - 3E(1/3ML)$, where the latter refer to the total energy of the slab with 1 ML of Cu, the slab alone, and the slab with 1/3 ML of Cu, respectively. We noted during our study that at 1 ML coverage, it was exothermic for OH to dissociate, placing the H well away from the remaining ad-O, which coordinates locally to two Cu atoms. This observation, however, does not affect the preference for wetting significantly (Table II).

It thus appears possible not only to increase the dispersion of ad-metal particles by hydroxylation [2, 28], but also to alter the growth mode completely if sufficient OH density is present [29]. It is of course possible that this surfactant effect extends to other impurities as well.

Acknowledgment

References

[1] P. Hohenberg and W. Kohn, *Phys. Rev.,* 1964, **136**, B864; W. Kohn and L. J. Sham, *Phys. Rev.*, 1965, **140**, A1133.
[2] G. Ertl and H.-J. Freund, *Phys. Today*, 1999, **52**, 32, and references therein.

[3] H.-J. Freund, H. Kuhlenbeck and V. Staemmler, *Rep. Prog. Phys.*, 1996, **59**, 283.

[4] R. M. Jaeger, *et al.*, *Surf. Sci.*, 1991, **259**, 235.

[5] C. Becker, *et al.*, *J. Vac. Sci. Technol.*, 1998, **A16**, 1000.

[6] R. J. Behm, *et al.*, to be published.

[7] O. Dulub, W. Hebenstreit, and U. Diebold, to be published.

[8] J. Libuda, *et al.*, *Surf. Sci.*, 1994, **318**, 61.

[9] S. Nepijko, M. Klimenkov, H. Kuhlenbeck, R. Schlögl, and H.-J. Freund, to be published.

[10] D. R. Jennison, C. Verdozzi, P. A. Schultz, and M. P. Sears, *Phys. Rev. B*, 1999, **59**, R15605.

[11] F. Winkelmann, et al., *Surf. Sci.*, 1994, **307-309**, 1148.

[12] *Adsorption on Ordered Surfaces of Ionic Solids and Thin Films*, H.-J. Freund and E. Umbach, eds. (Springer-Verlag, 1993).

[13] P. A. Thiel and T. E. Madey, *Surf. Sci. Rep.*, 1987, **7**, 211.

[14] G. Haas, A. Menck, H. Brune, J. V. Barth, J. A. Venables, and K. Kern, to be published.

[15] M. J. Stirniman, C. Huang, R. S. Smith, S. A. Joyce, and B. D. Kay, *J. Chem. Phys.*, 1996, **105**, 1295.

[16] J. Günster, J. Stultz, S. Krischok, D. W. Goodman, P. Stracke, and V. Kempter, to be published.

[17] U. Diebold, et al., *Surf. Sci.*, 1998, **411**, 137.

[18] A. Bogicevic and D. R. Jennison, *Surf. Sci.*, in press.

[19] J. Ahn and J. W. Rabalais, *Surf. Sci.*, 1997, **388**, 121.

[20] C. Verdozzi, et al., *Phys. Rev. Lett.*, 1999, **82**, 799, and references therein.

[21] A. Bogicevic and D. R. Jennison, *Phys. Rev. Lett.*, 1999, **82**, 4050.

[22] S. Varma, G. S. Chottiner, and M. Arbab, *J. Vac. Sci. Technol.*, 1992, **A10**, 2857.

[23] J. G. Chen, M. L. Colaianni, W. H. Weinberg and J. T. Yates, Jr., *Surf. Sci.*, 1992, **279**, 223.

[24] F. S. Ohuchi, R. H. French and R. V. Kasowski, *J. Appl. Phys.*, 1987, **62**, 2286.

[25] Y. Wu, E. Garfunkel and T. E. Madey, *J. Vac. Science and Technol.*, 1996, **A14**, 1662.

[26] S. Gota, M. Gautier, L. Douillard, N. Thromat, J. P. Duraud, and P. Le Fevre, *Surf. Sci.*, 1995, **323**, 163; see also M. Gautier, L. Pham Van and J. P. Duraud, *Europhys. Lett.*, 1992, **18**, 175.

[27] M. Gautier, J. P. Duraud and L. Pham Van, *Surf. Sci. Lett.*, 1991, **249**, L327.

[28] J. Libuda, *et al.*, *Surf. Sci.*, 1997, **384**, 106.

[29] J. A. Kelber, *et al.*, *Surf. Sci.* (submitted).

[30] G. Kresse and J. Hafner, *Phys. Rev. B*, 1993, **47**, 558; 1994, **49**, 14251; 1996, **54**, 11169.

[31] D. Vanderbilt, *Phys. Rev. B*, 1985, **32**, 8412; 1990, **41** 7892.

[32] J. P. Perdew and A. Zunger, *Phys. Rev. B*, 1981, **23**, 5048; D. M. Ceperley and B. J. Alder, *Phys. Rev. Lett.*, 1980, **45**, 566.

[33] J. P. Perdew, *et al.*, *Phys. Rev. B*, 1992, **46**, 6671.

[34] Y. Yourdshahyan, *et al.*, *Phys. Rev. B*, 1997, **55**, 8721.

[35] Y. Yourdshahyan, *et al.*, *Applied Physics Report* 99-1, submitted; B. Holm, *et al.*, *Phys. Rev. B.*, 1999, **59**, 12777.

[36] See, for example, M. A. Johnson, *et al.*, *J. Phys. Chem.*, 1999, **103**, 3391, and references therein.

Tables

t/o ratio (%), type	0, pure *o*	50, zig-zag	50, stripe	100, pure *t*
Unit cell	1x1	2x1	3x1	1x1
Ru(0001)	1.2	0.0	0.5	1.0
Al(111)	1.8	0.0	—	1.6

Table I. Relative energies in eV (per Al_2O_3 unit) vs. the Al-ion tetrahedral/octahedral site ratio for 5 Å alumina films on Ru and Al substrates. (The striped structure on Al(111) has not yet been studied.)
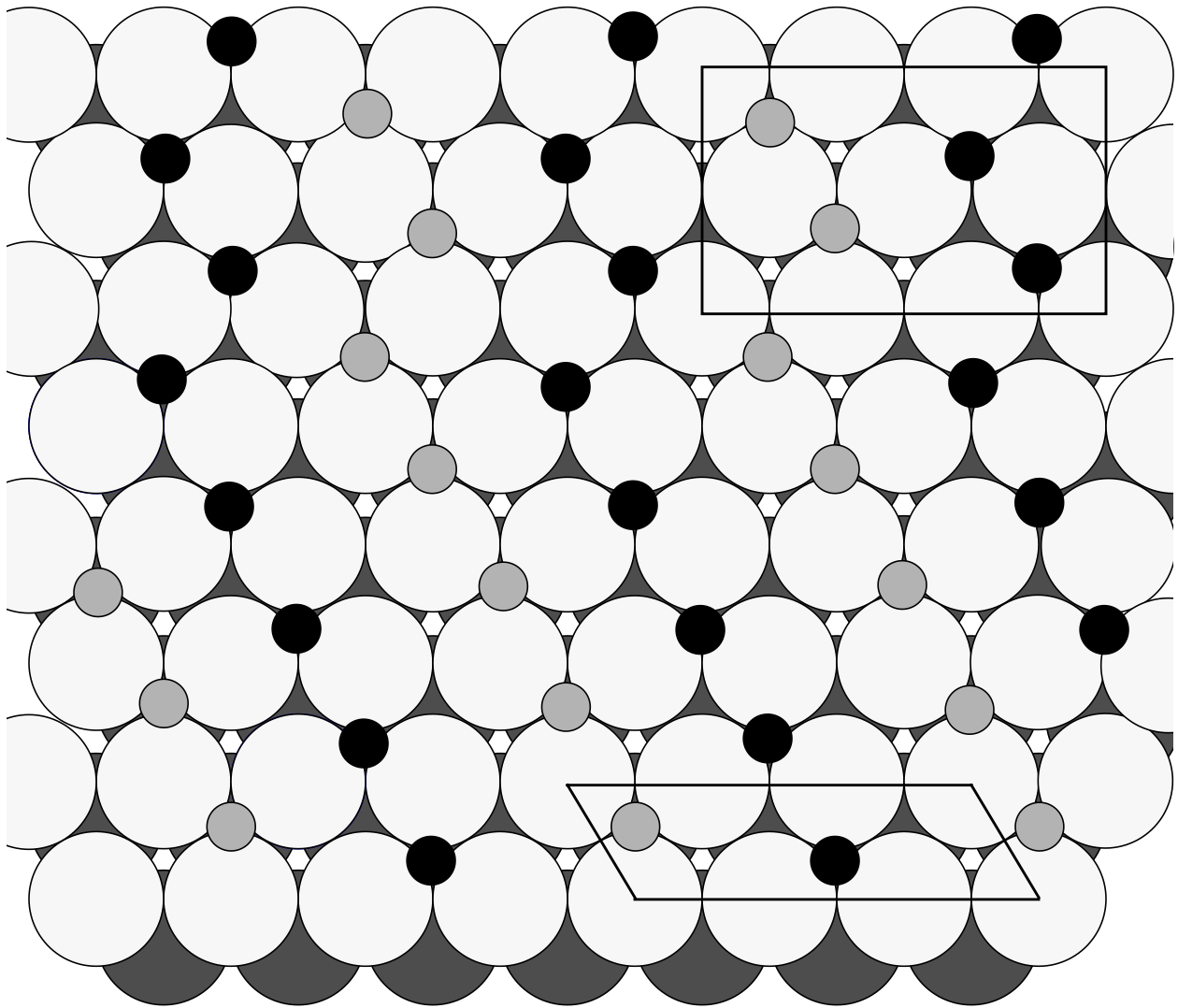
Cu Coverage:	1/3 ML	1 ML	ΔE
sapphire:	1.8	0.5	-4.5
sapphire+OH	5.2	1.1	+3.8
sapphire+O+H	—	1.3	+3.1

Table II. The LDA adsorption energy of Cu on a per atom basis in eV on clean sapphire(0001) and on hydroxylated sapphire (1/3 ML of ad-OH). With 1 ML of Cu, it was also found exothermic for Cu to dissociate the OH, as shown. The Born-Haber energy ΔE is positive when wetting occurs.
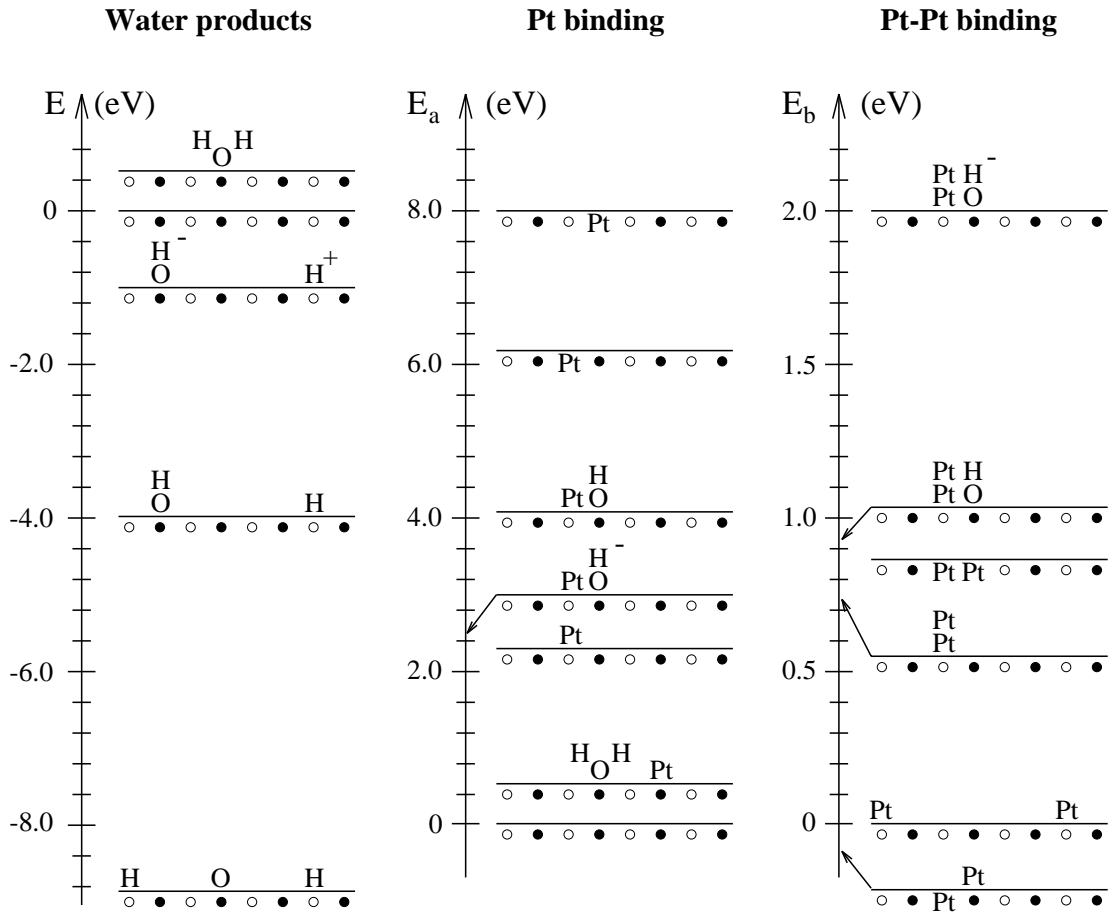
Figure Captions:

Fig. 1 The preferred structure of the thin film has alternating rows of tetrahedral and octahedral site Al-ions in a zig-zag pattern (top) rather than the striped pattern (bottom). The large spheres are O-ions, the small spheres Al-ions, in either octahedral (black) or tetrahedral (gray) sites.

Fig. 2 Pt adsorption, Pt_2 binding energy, and relative stability of water products on MgO(100) and in the presence of surface defects. The open circles under each line denote O ions, the filled circles Mg ions. Negative energies indicate metastable adsorption with respect to (i) isolated gas phase H_2O molecule, (ii) isolated gas phase Pt atom, and (iii) two isolated Pt adatoms, for the three panels respectively.

Zig-Zag (top) going to Stripe (bottom).

Water products   **Pt binding**   **Pt-Pt binding**

Jennison — Figure 2